1 R-Z Geometry

Solving the transport equation in different coordinate systems may provide simpler ways of modeling a particular geometry or symmetry. In this section, we derive the R-Z transport equation to be solved. It assumes there is no variation in the azimuthal direction (of a cylinder), hence problems in R-Z geometry look very similar to problems in X-Y geometry. The streaming operator in cylindrical geometry is [**?**]

$$\mathbf{\Omega} \cdot \boldsymbol{\nabla}\psi = \frac{\mu}{r}\frac{\partial}{\partial r}(r\psi) + \frac{\eta}{r}\frac{\partial \psi}{\partial \zeta} + \xi\frac{\partial \psi}{\partial z} - \frac{1}{r}\frac{\partial}{\partial \omega}(\eta\psi), \tag{1}$$

where $\mathbf{\Omega}$ is the direction of travel unit vector, ψ is the angular flux, and

$$\mu \equiv \mathbf{\Omega} \cdot \hat{e}_r = \sqrt{1-\xi^2}\cos\omega = \sin(\theta)\cos(\omega), \tag{2}$$

$$\eta \equiv \mathbf{\Omega} \cdot \hat{e}_\theta = \sqrt{1-\xi^2}\sin\omega = \sin(\theta)\sin(\omega), \tag{3}$$

$$\xi \equiv \mathbf{\Omega} \cdot \hat{e}_z = \cos(\theta). \tag{4}$$

The variables μ, η, ξ, ω, and θ are shown in the cylindrical coordinate system in Figure 1. We assume there is no solution variation in the azimuthal direction, i.e.

$$\frac{\partial \psi}{\partial \zeta} \equiv 0, \tag{5}$$

which simplifies the streaming term to

$$\mathbf{\Omega} \cdot \boldsymbol{\nabla}\psi = \frac{\mu}{r}\frac{\partial}{\partial r}(r\psi) + \xi\frac{\partial \psi}{\partial z} - \frac{1}{r}\frac{\partial}{\partial \omega}(\eta\psi). \tag{6}$$

The transport equation in R-Z geometry is then

$$\begin{aligned}\frac{\mu}{r}\frac{\partial}{\partial r}r\psi\left(r,z,\mathbf{\Omega}\right) + \xi\frac{\partial}{\partial z}\psi\left(r,z,\mathbf{\Omega}\right) - \frac{1}{r}\frac{\partial}{\partial \omega}\eta\psi\left(r,z,\mathbf{\Omega}\right) + \sigma_t\left(r,z\right)\psi\left(r,z,\mathbf{\Omega}\right) \\ = \frac{1}{4\pi}\int_{4\pi}\sigma_s\left(r,z\right)I\left(r,z,\mathbf{\Omega}'\right)d\Omega' + S_0\left(r,z,\mathbf{\Omega}\right)\end{aligned} \tag{7}$$

where σ_t is the total cross section, σ_s is the scattering cross section, and S_0 is an isotropic source as before.

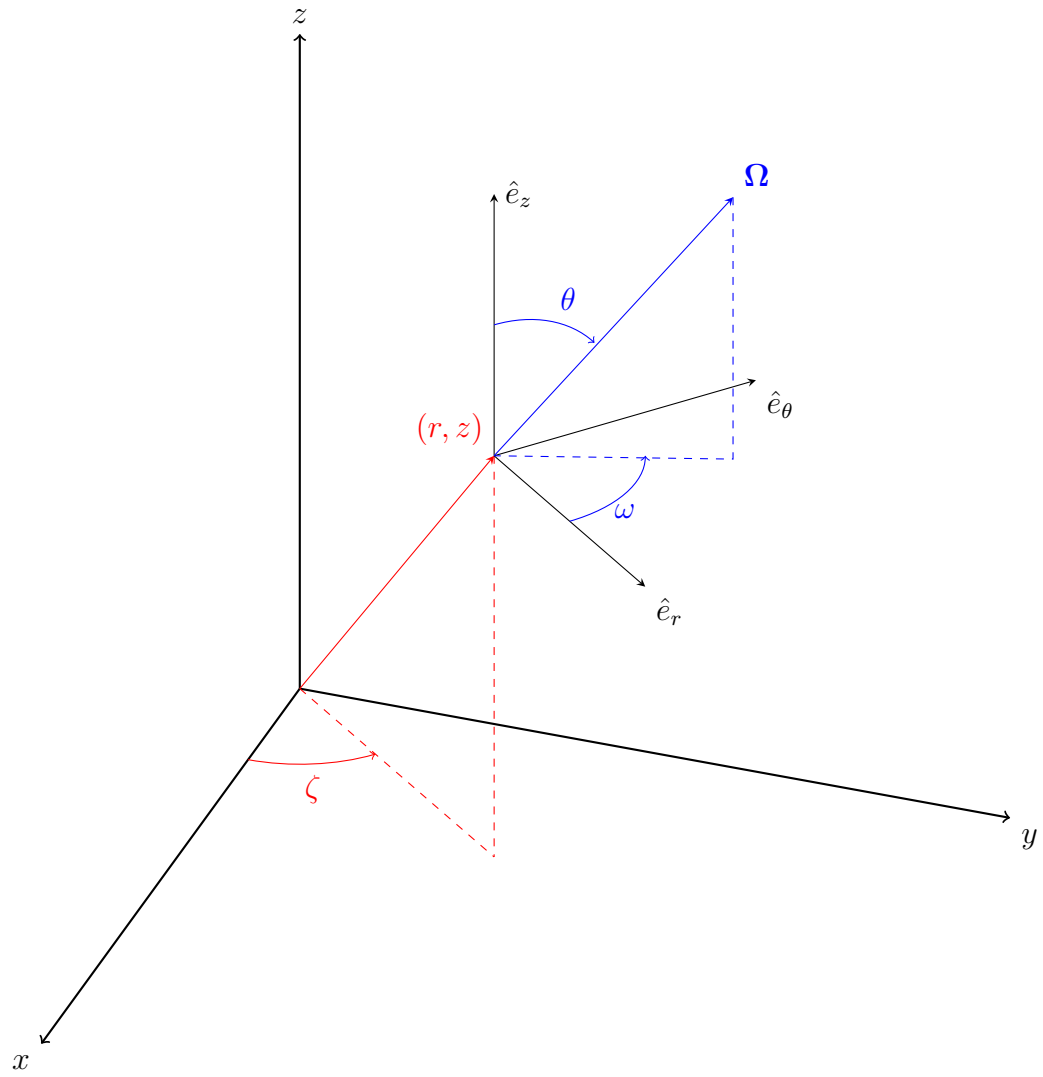

Figure 1: Cylindrical space-angle coordinate system showing the position (r, z) and direction of travel $\boldsymbol{\Omega}$.

1.1 Angular Discretization

Discretizing Equation 7 with a level-symmetric angular quadrature results in

$$\frac{\mu_{n,m}}{r}\frac{\partial}{\partial r}r\psi_{n,m}\left(r,z\right)+\xi_n\frac{\partial}{\partial z}\psi_{n,m}\left(r,z\right)-\frac{1}{r}\frac{\partial}{\partial\omega}\eta_{n,m}\psi_{n,m}\left(r,z\right)+\sigma_t\left(r,z\right)\psi_{n,m}\left(r,z\right)$$
$$=\frac{1}{4\pi}\int_{4\pi}\sigma_s\left(r,z\right)I\left(r,z,\boldsymbol{\Omega}'\right)d\Omega'+S_0\left(r,z,\boldsymbol{\Omega}\right) \quad (8)$$

for direction $\boldsymbol{\Omega}_{n,m}$, where index n describes a level of quadrature with constant ξ and the m index denotes the quadrature point on that level. The (n, m) indexing is shown

in Figure 2.

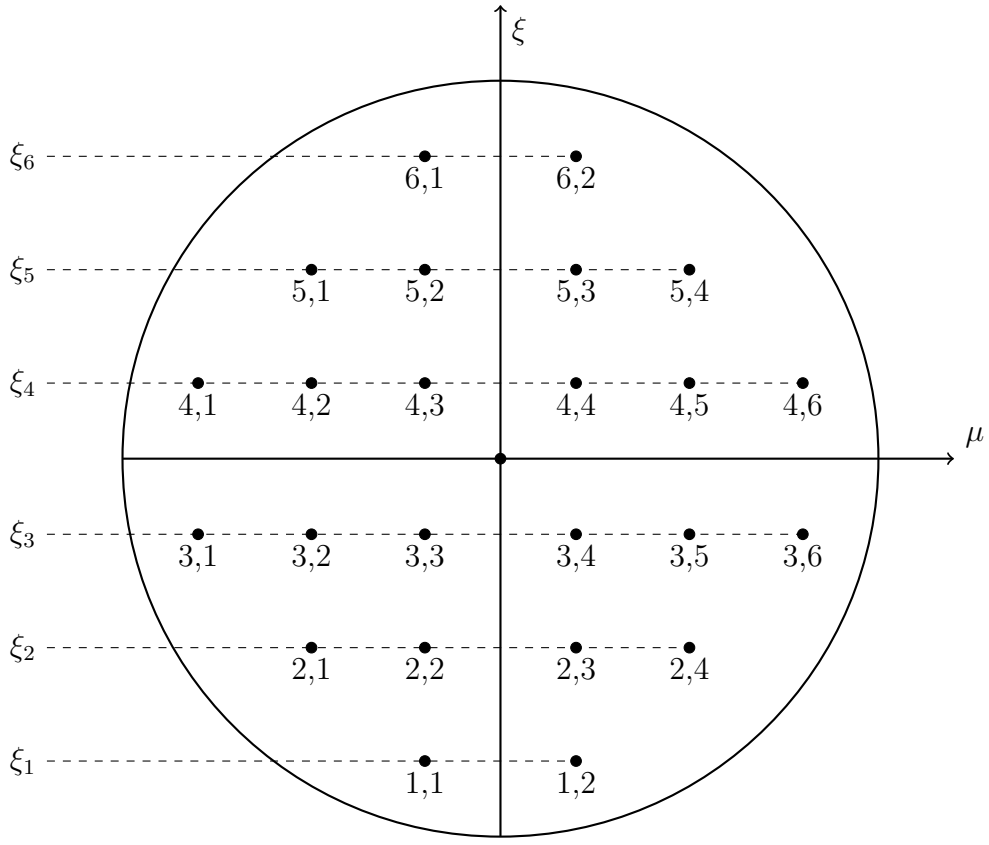

Figure 2: Angular discretization showing (ξ, μ) pairs; adapted from [**?**]

One of the major challenges is handling the anglar derivative term. Lewis and Miller [**?**] describes an approximation for the partial derivative of the intensity with respect to ω:

$$-\frac{1}{r}\frac{\partial}{\partial\omega}\eta_{m,n}\psi_{n,m}\left(r,z\right) = \frac{\alpha^n_{m+1/2}\psi_{n,m+1/2}(r,z) - \alpha^n_{m-1/2}\psi_{n,m-1/2}(r,z)}{rw_{n,m}} \tag{9}$$

where $\alpha^n_{m+1/2}$ and $\alpha^n_{m-1/2}$ are angular differencing coefficients, and $w_{n,m}$ is the angular

quadrature weight. We substitute this into Equation 18,

$$\frac{\mu_{n,m}}{r}\frac{\partial}{\partial r}r\psi_{n,m}\left(r,z\right)+\xi_n\frac{\partial}{\partial z}\psi_{n,m}\left(r,z\right) + \frac{\alpha^n_{m+1/2}\psi_{m+1/2,n}(r,z)-\alpha^n_{m-1/2}\psi_{m-1/2,n}(r,z)}{rw_{n,m}}+\sigma_t\left(r,z\right)\psi_{n,m}\left(r,z\right) = \frac{1}{4\pi}\int_{4\pi}\sigma_s\left(r,z\right)\psi\left(r,z,\mathbf{\Omega}'\right)d\Omega'+\frac{1}{4\pi}S_0\left(r,z\right) \quad (10)$$

Here, we pause to notice that there are similarities and differences between our Cartesian discretization. The absorption term, axial derivative term, and right-hand-side are the same in both coordinate systems. The differences arise in the radial and angular derivative terms.

After multiplying through by the radius r, the radial derivative term has a factor of r inside the derivative. The angular derivative term is also new and does not resemble a mass matrix so MFEM will require additional modification.

Requiring Equation 10 to satisfy the uniform infinite medium solution results in the condition,

$$\alpha^n_{m+1/2}=\alpha^n_{m-1/2}-\mu_{n,m}w_{n,m} \quad (11)$$

If $\alpha^n_{1/2}$ is known, then the remaining coefficients are uniquely determined. To find $\alpha^n_{1/2}$, we require that Equation 10 satisfy the conservation equation (Eq. 7). Given a quadrature set with an even number of $\mu_{n,m}$ values, setting $\alpha^n_{1/2}=0$ results in $\alpha^n_{M_n+1/2}=0$ per Equation 11 and the conservation equation is satisfied.

A relationship between $\psi_{n,m}$, $\psi_{n,m+1/2}$, and $\psi_{n,m-1/2}$ must be established. A weighted diamond difference scheme has been established by Morel and Montry [**?**],

$$\psi_{n,m}(r,z)=\tau_{n,m}\psi_{n,m+1/2}+\left(1-\tau_{n,m}\right)\psi_{n,m-1/2} \quad (12)$$

where $\tau_{n,m}$ linearly interpolates μ:

$$\tau_{n,m}=\frac{\mu_{n,m}-\mu_{n,m-1/2}}{\mu_{n,m+1/2}-\mu_{n,m-1/2}} \quad (13)$$

with

$$\mu_{n,m+1/2} = \sqrt{1-\xi_n^2}\cos\left(\varphi_{n,m+1/2}\right) \tag{14}$$

$$\varphi_{n,m+1/2} = \varphi_{n,m-1/2} + \pi\frac{w_{n,m}}{w_n} \tag{15}$$

$$w_n = \sum_{m=1}^{M_n} w_{n,m} \tag{16}$$

We take Equation 10, multiply through by r and perform a product rule on the radial derivative term,

$$\begin{aligned}\mu_{n,m}\left[\psi_{n,m}(r,z) + r\frac{\partial}{\partial r}\psi_{n,m}(r,z)\right] + r\xi_n\frac{\partial}{\partial z}\psi_{n,m}(r,z) \\ + \frac{\alpha^n_{m+1/2}\psi_{m+1/2,n}(r,z) - \alpha^n_{m-1/2}\psi_{m-1/2,n}(r,z)}{w_{n,m}} + r\sigma_t(r,z)\,\psi_{n,m}(r,z) \\ = \frac{r}{4\pi}\int_{4\pi}\sigma_s(r,z)\,\psi(r,z,\mathbf{\Omega}')\,d\Omega' + \frac{r}{4\pi}S_0(r,z).\end{aligned} \tag{17}$$

We solve Equation 12 for $\psi_{n,m+1/2}$, perform a substitution, and move the known quantities to the right-hand-side,

$$\begin{aligned}\mu_{n,m}r\frac{\partial}{\partial r}\psi_{n,m}(r,z) + r\xi_n\frac{\partial}{\partial z}\psi_{n,m}(r,z) + \mu_{n,m}\psi_{n,m}(r,z) \\ + \frac{\alpha^n_{m+1/2}}{\tau_{n,m}w_{n,m}}\psi_{n,m}(r,z) + r\sigma_t(r,z)\,\psi_{n,m}(r,z) \\ = \frac{r}{4\pi}\int_{4\pi}\sigma_s(r,z)\,\psi(r,z,\mathbf{\Omega}')\,d\Omega' + \frac{r}{4\pi}S_0(r,z) \\ + \left(\frac{1-\tau_{n,m}}{\tau_{n,m}}\frac{\alpha^n_{m+1/2}}{w_{n,m}} + \frac{\alpha^n_{m-1/2}}{w_{n,m}}\right)\psi_{n,m-1/2}(r,z).\end{aligned} \tag{18}$$

Given a level-symmetric quadrature set, all of the $\alpha^n_{n,m\pm1/2}$ and $\tau_{n,m}$ values can be computed. We solve the starting direction equation to obtain $\psi_{n,1/2}$. That is, we solve the X-Y system for directions $\mathbf{\Omega}_{n,1/2}$,

$$\mathbf{\Omega}_{n,1/2}\cdot\boldsymbol{\nabla}\psi_{n,1/2} + \sigma_t\psi_{n,1/2} = \frac{1}{4\pi}\sigma_s\phi + \frac{1}{4\pi}S_0 \tag{19}$$

There is an alternate angular discretization method developed by Warsa and Prinja [**?**]. Instead of finding an approximation for the angular derivative, they per-

form a product rule:

$$\frac{\partial\psi}{\partial\omega} \equiv \frac{\partial\mu}{\partial\omega}\frac{\partial\psi}{\partial\mu} \tag{20}$$

Since,

$$\frac{\partial\mu}{\partial\omega} \equiv -\xi, \tag{21}$$

The angular derivative can be written

$$\frac{\partial\psi}{\partial\omega} \equiv -\xi\frac{\partial\psi}{\partial\mu} \tag{22}$$

Here, an approximation for the μ-derivative must be established.

1.2 Spatial Discretization

The finite element discretization is performed here. The methodology is similar to the Cartesian geometry. First, we subdivide a problem domain using a spatial mesh. Then, we multiply Equation 18 by a test function and integrate over the volume of a single mesh zone,

$$\begin{aligned}(r\boldsymbol{\Omega}_{n,m}\cdot\boldsymbol{\nabla}\psi_{n,m}, v_i)_{\mathbb{D}} + (\mu_{n,m}\psi_{n,m}, v_i)_{\mathbb{D}} \\ + \left(\frac{\alpha^n_{m+1/2}}{\tau_{n,m}w_{n,m}}\psi_{n,m}, v_i\right)_{\mathbb{D}} + (r\sigma_t\psi_{n,m}, v_i)_{\mathbb{D}} \\ = \left(\frac{r}{4\pi}\int_{4\pi}\sigma_s\psi d\Omega', v_i\right)_{\mathbb{D}} + \left(\frac{r}{4\pi}S_0, v_i\right)_{\mathbb{D}} \\ + \left(\left(\frac{1-\tau_{n,m}}{\tau_{n,m}}\frac{\alpha^n_{m+1/2}}{w_{n,m}} + \frac{\alpha^n_{m-1/2}}{w_{n,m}}\right)\psi_{n,m-1/2}, v_i\right)_{\mathbb{D}},\end{aligned} \tag{23}$$

where the Cartesian gradient operator is used and the inner product notation,

$$(a,b)_{\mathbb{D}} \equiv \int_{\mathbb{D}} ab, \tag{24}$$

is used. We perform an integration by parts,

$$\begin{aligned}(r\mathbf{\Omega}_{n,m}\cdot\hat{n}\psi_{n,m},v_i)_{\partial\mathbb{D}}-(r\psi_{n,m},\mathbf{\Omega}_{n,m}\cdot\boldsymbol{\nabla}v_i)_{\mathbb{D}}+(\mu_{n,m}\psi_{n,m},v_i)_{\mathbb{D}}\\ +\left(\frac{\alpha^n_{m+1/2}}{\tau_{n,m}w_{n,m}}\psi_{n,m},v_i\right)_{\mathbb{D}}+(r\sigma_t\psi_{n,m},v_i)_{\mathbb{D}}\\ =\left(\frac{r}{4\pi}\int_{4\pi}\sigma_s\psi d\Omega',v_i\right)_{\mathbb{D}}+\left(\frac{r}{4\pi}S_0,v_i\right)_{\mathbb{D}}\\ +\left(\left(\frac{1-\tau_{n,m}}{\tau_{n,m}}\frac{\alpha^n_{m+1/2}}{w_{n,m}}+\frac{\alpha^n_{m-1/2}}{w_{n,m}}\right)\psi_{n,m-1/2},v_i\right)_{\mathbb{D}},\end{aligned}\tag{25}$$

to obtain our angular and spatially discretized R-Z transport equation.

WE PERFORMED SOME STUDIES TO MAKE SURE IT'S RIGHT...

We first solved a uniform infinite medium problem with $\sigma_t = 1.0$, $\sigma_s = 0.3$, and $S_0 = 0.7$ for 1^{st}-order FEM on a 2^{nd}-order mesh using S_4 level-symmetric angular quadrature. The solution, shown in Figure 3, demonstrates we get the exact flat solution of $\phi = 1.0$.

We tested several MMS problems as well. First, we defined the manufactured solution

$$\psi = (1-\mu^2)(1-\xi^2)\sin\left(\frac{\pi}{2}r\right)\cos(\pi z)\tag{26}$$

with 2^{nd}-order FEM, Orthogonal quadrilateral mesh, $\sigma_t = 1.0$, $\sigma_s = 0.3$, $S_0 = 0.7$, S_4 level-symmetric angular quadrature. The solution is shown in Figure 4 and the L^2-error was 0.132.

Removing the angular dependence in the manufactured solution,

$$\psi = \sin\left(\frac{\pi}{2}r\right)\cos(\pi z),\tag{27}$$

increased the accuracy of our DGFEM approximation. Shown in Figure 5, the L^2-error was reduced to 4.59×10^{-5}.

Bailey et al. [**?**] showed 2^{nd}-order convergence using PWLD and BLD using the

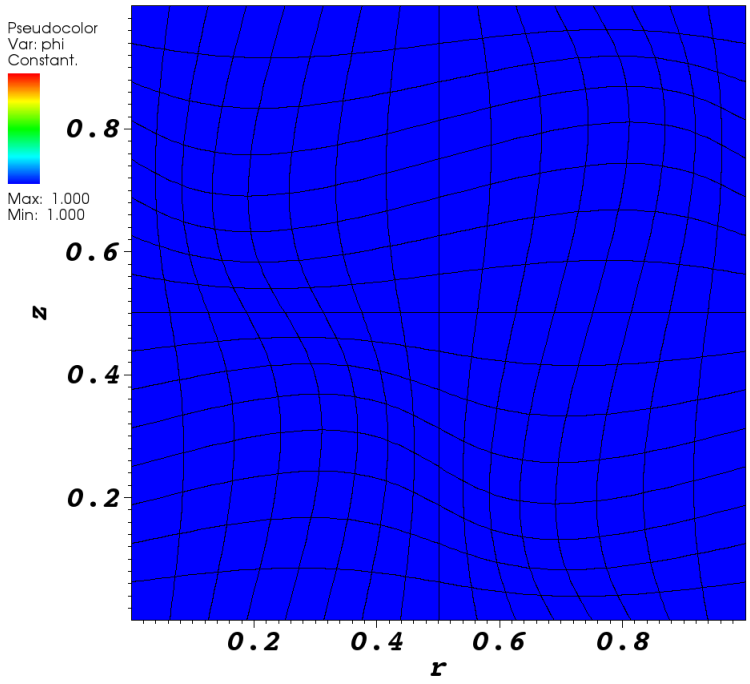

Figure 3: Uniform infinite medium solution.

manufactured solution

$$\psi_{\text{MMS}}(r, z) = (\sin(\pi r) + 1 - r)\sin(\pi z), \tag{28}$$

for $\sigma_t = 3\ \text{cm}^{-1}$ and $\sigma_s = 0.9999\sigma_t$. We solved this same problem using $p = \{1, 2, 4, 6, 8\}$ on an orthogonal and 2^{nd}-order curved mesh using S_8 level-symmetric angular quadrature. The incident angular flux is equal to Equation 28. Figure 6 shows the $p = 2$ solution on a 2^{nd}-order mesh.

The spatial convergence study performed by Bailey et al. demonstrated 2^{nd}-order converge for their 1^{st}-order methods. Figures 7a and 7b demonstrate $O(p + 1)$ convergence on an orthogonal mesh and 2^{nd}-order mesh, respectively. Reference lines are also provided for comparison.

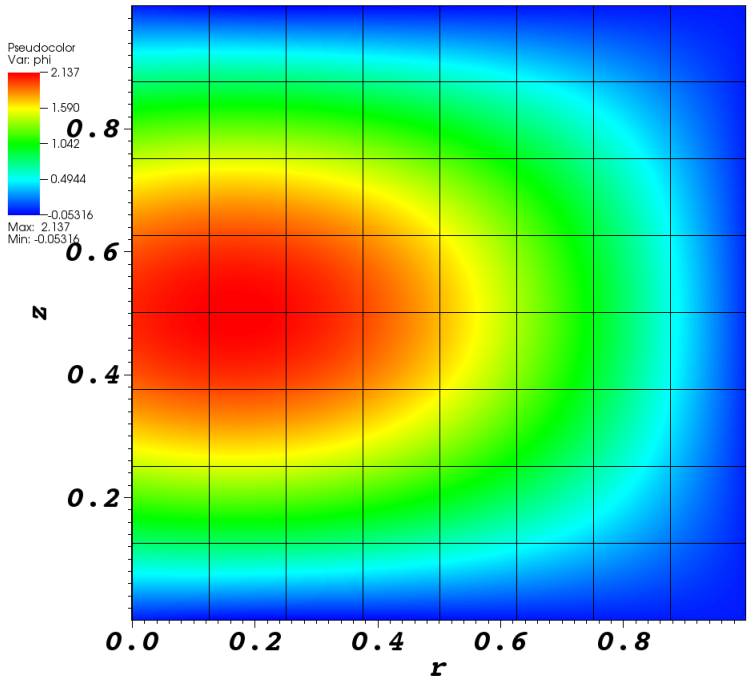

Figure 4: MMS solution for Equation 26.

1.3 Lumping

1.4 Diffusion Synthetic Acceleration

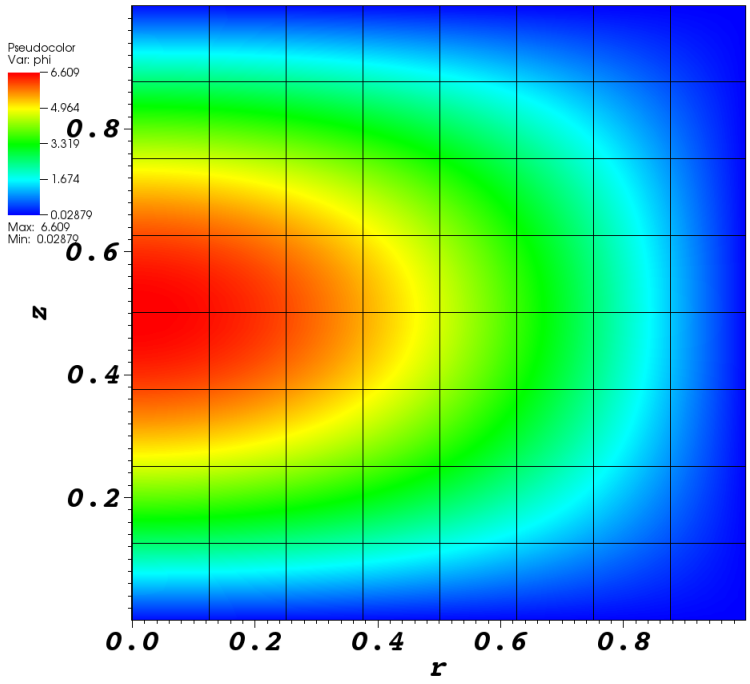

Figure 5: MMS solution for Equation 27.

1.5 Symmetry Preservation

We want R-Z geometry to solve and preserve 1-dimensional spherical solutions. The transport equation in spherical geometry is

$$\mathbf{\Omega}\cdot\mathbf{\nabla}\psi = \frac{\partial\psi}{\partial r}\mathbf{\Omega}\cdot\mathbf{\nabla}r + \frac{\partial\psi}{\partial\mu}\mathbf{\Omega}\cdot\mathbf{\nabla}\mu \tag{29}$$

$$= \mu\frac{\partial\psi}{\partial r} + \frac{(1-\mu^2)}{r}\frac{\partial\psi}{\partial\mu} \tag{30}$$

$$= \frac{\mu}{r^2}\frac{\partial}{\partial r}(r^2\psi) + \frac{\partial}{\partial\mu}\frac{[(1-\mu^2)\psi]}{r} \tag{31}$$

$$\mu\frac{\partial}{\partial r}(r^2\psi) + r\frac{\partial}{\partial\mu}((1-\mu^2)\psi) + r^2\sigma_t\psi = \frac{1}{4\pi}\sigma_s\phi + \frac{1}{4\pi}S_0. \tag{32}$$

In 1-dimensional geometry, this simplifies to

$$\mu\frac{\partial\psi}{\partial r} + \sigma_t\psi = \frac{1}{4\pi}\sigma_s\phi + \frac{1}{4\pi}S_0. \tag{33}$$

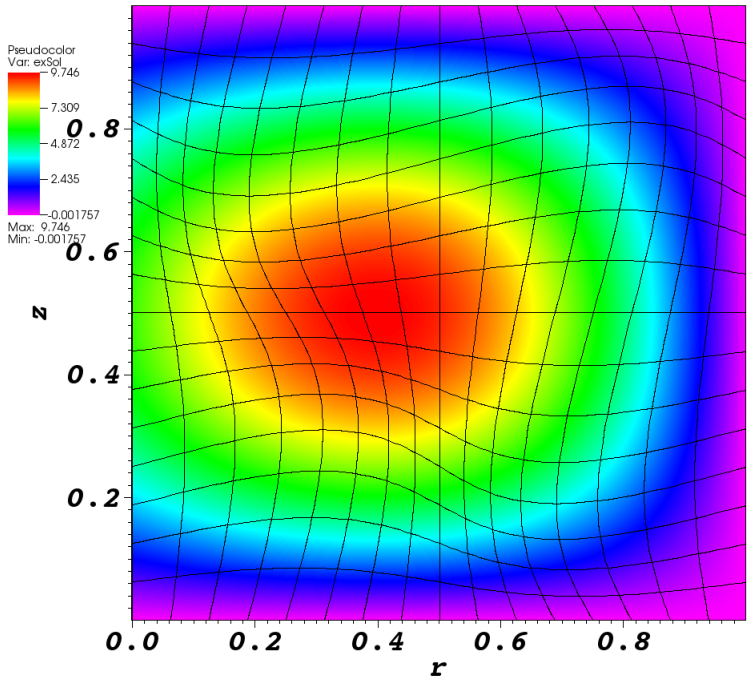

Figure 6: MMS solution to Equation 28.

We can solve this for ψ.

$$\frac{\partial \psi(r)}{\partial r} e^{\sigma_t r/\mu} + \frac{\sigma_t}{\mu} \psi(r) e^{\sigma_t r/\mu} = \frac{1}{4\pi\mu} \left(\sigma_s \phi + S_0\right) e^{\sigma_t r/\mu} \tag{34}$$

$$\frac{\partial}{\partial r} \left(\psi(r) e^{\sigma_t r/\mu}\right) = \frac{1}{4\pi\mu} \left(\sigma_s \phi + S_0\right) e^{\sigma_t r/\mu} \tag{35}$$

$$\int \frac{\partial}{\partial r'} \left(\psi(r') e^{\sigma_t r'/\mu}\right) dr' = \frac{1}{4\pi\mu} \int \left(\sigma_s \phi(r') + S_0\right) e^{\sigma_t r'/\mu} dr' \tag{36}$$

$$\psi(r) e^{\sigma_t r/\mu} - c = \frac{1}{4\pi\mu} \int \left(\sigma_s \phi(r') + S_0\right) e^{\sigma_t r'/\mu} dr' \tag{37}$$

$$\psi(r) = e^{-\sigma_t r/\mu} \frac{1}{4\pi\mu} \int \left(\sigma_s \phi(r') + S_0\right) e^{\sigma_t r'/\mu} dr' + c e^{-\sigma_t r/\mu} \tag{38}$$

$$\psi(1) = 1 = e^{-\sigma_t/\mu} \frac{1}{4\pi\mu} \int \left(\sigma_s \phi(r') + S_0\right) e^{\sigma_t r'/\mu} dr' + c e^{-\sigma_t/\mu} \tag{39}$$

$$c = e^{\sigma_t/\mu} - \frac{1}{4\pi\mu} \int \left(\sigma_s \phi(r') + S_0\right) e^{\sigma_t r'/\mu} dr' \tag{40}$$

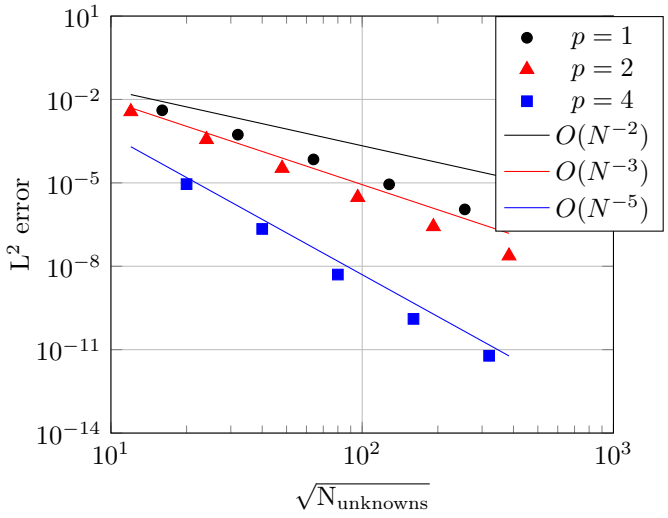

(a) Orthogonal quadrilateral mesh.

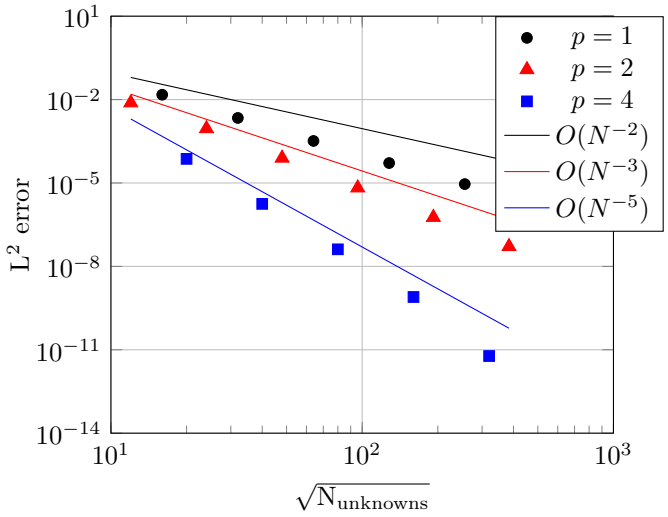

(b) 2[nd]-order curved mesh.

Figure 7: L^2-norm of the errors from the manufactured solution and reference lines, where $N_{\text{unknowns}} = N_{\text{cells}}(p+1)^2$.

$$\psi(r) = e^{-\sigma_t r/\mu}\frac{1}{4\pi\mu}\int (\sigma_s\phi(r') + S_0)\, e^{\sigma_t r'/\mu} dr' + \left[e^{\sigma_t/\mu} - \frac{1}{4\pi\mu}\int (\sigma_s\phi(r') + S_0)\, e^{\sigma_t r'/\mu} dr'\right] e^{-\sigma_t r/\mu} \quad (41)$$

$$\psi(r) = e^{-\sigma_t r/\mu}\frac{1}{4\pi\mu}\int (\sigma_s\phi(r') + S_0)\, e^{\sigma_t r'/\mu} dr' + e^{(1-r)\sigma_t/\mu} - e^{-\sigma_t r/\mu}\frac{1}{4\pi\mu}\int (\sigma_s\phi(r') + S_0)\, e^{\sigma_t r'/\mu} dr' \quad (42)$$

$$\psi(r) = e^{(1-r)\sigma_t/\mu} \tag{43}$$

We use MMS to solve a 1-D spherical problem using the R-Z geometry spatial discretization. The manufactured solution is

$$\psi_{\text{MMS}}(\rho) = \sin(\pi\rho) + 2 - \rho, \tag{44}$$

where $\rho = \sqrt{r^2 + z^2}$ is the distance from the origin (i.e. the spherical radius). Plugging this into the R-Z transport equation,

$$\begin{aligned}\frac{\mu}{r}\frac{\partial}{\partial r}\left[r\left(\sin(\pi\rho) + 2 - \rho\right)\right] + \frac{\eta}{r}\frac{\partial}{\partial r}\left(\sin(\pi\rho) + 2 - \rho\right) + \xi\frac{\partial}{\partial z}\left(\sin(\pi\rho) + 2 - \rho\right) \\ - \frac{1}{r}\frac{\partial}{\partial \omega}\left[\eta\left(\sin(\pi\rho) + 2 - \rho\right)\right] + \sigma_t\left(\sin(\pi\rho) + 2 - \rho\right) \\ = \frac{1}{2\pi}\sigma_s\phi_{\text{MMS}} + \frac{1}{2\pi}S_0. \end{aligned} \tag{45}$$

Integrating ψ_{MMS} over all directions reveals ϕ_{MMS},

$$\begin{aligned}\frac{\mu}{r}\frac{\partial}{\partial r}\left[r\left(\sin(\pi\rho) + 2 - \rho\right)\right] + \frac{\eta}{r}\frac{\partial}{\partial r}\left(\sin(\pi\rho) + 2 - \rho\right) + \xi\frac{\partial}{\partial z}\left(\sin(\pi\rho) + 2 - \rho\right) \\ - \frac{1}{r}\frac{\partial}{\partial \omega}\left[\eta\left(\sin(\pi\rho) + 2 - \rho\right)\right] + \sigma_t\left(\sin(\pi\rho) + 2 - \rho\right) \\ = \sigma_s\left(\sin(\pi\rho) + 2 - \rho\right) + \frac{1}{2\pi}S_0. \end{aligned} \tag{46}$$

We perform some simplifications,

$$\begin{aligned}\frac{\mu}{r}\frac{\partial}{\partial r}\left[r\left(\sin(\pi\rho) + 2 - \rho\right)\right] + \frac{\eta}{r}\frac{\partial}{\partial r}\left(\sin(\pi\rho) + 2 - \rho\right) + \xi\frac{\partial}{\partial z}\left(\sin(\pi\rho) + 2 - \rho\right) \\ - \frac{1}{r}\frac{\partial}{\partial \omega}\left[\eta\left(\sin(\pi\rho) + 2 - \rho\right)\right] + \sigma_t\left(\sin(\pi\rho) + 2 - \rho\right) \\ = \sigma_s\left(\sin(\pi\rho) + 2 - \rho\right) + \frac{1}{2\pi}S_0. \end{aligned} \tag{47}$$

Because of the angular derivative in the streaming term, we reduce the influence of the direction dependence as much as possible by using higher order level-symmetric angular quadrature.

We evaluate the relative asymmetry by calculating the averages of all nodes at each ρ value and

$$\phi_{\text{sym}}(\rho,\theta) = \frac{\phi_{\text{code}}(\rho,\theta) - \phi_{\text{avg}}(\rho)}{\phi_{\text{avg}}(\rho)}, \tag{48}$$

where

$$\phi_{\text{avg}}(\rho) = \frac{1}{N_{\text{nodes}}(\rho)} \sum_{i=1}^{N_{\text{nodes}}(\rho)} \phi(\rho,\theta_i) \tag{49}$$

is the average scalar flux at all nodes at the same spherical radius ρ.

1.6 Other

1.7 Material Discontinuity Stress Test

We adapted this problem from Palmer [**?**] and solved it without DSA in Woods et al. [**?**]. There are five different material regions described in Table 1 and Figure 8.

Table 1: Material discontinuity stress test with MIP DSA material properties.

Material Region	σ_t cm^{-1}	σ_s cm^{-1}	S_0 cm^{-2} s^{-1}
Source	1.0	1.0	1.0
Very thin absorber	0.0001	0.0	0.0
Thick absorber	10.0	0.0	0.0
Very thick absorber	100.0	0.0	0.0
Very thick scatterer	1000.0	1000.0	0.0

This problem has opacities that range several orders of magnitude, resulting in strong material discontinuities. We also introduce anisotropic incident intensities into the scattering region by preferentially attenuating intensities that are not perpendicular to the thick absorber. We expect some degradation in the DSA in problems with

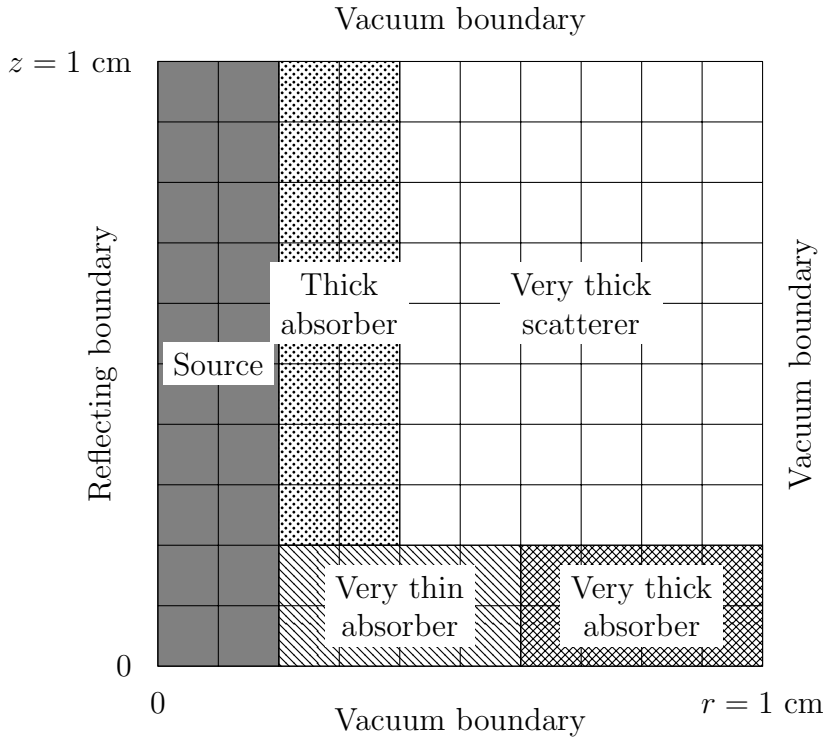

Figure 8: Material discontinuity stress test with MIP DSA problem geometry; materials defined in Table 1.

strong material discontinuities [?]. We also expect boundary layers to form from the anisotropic incident intensities [?]. The solution is shown in Figure 9.

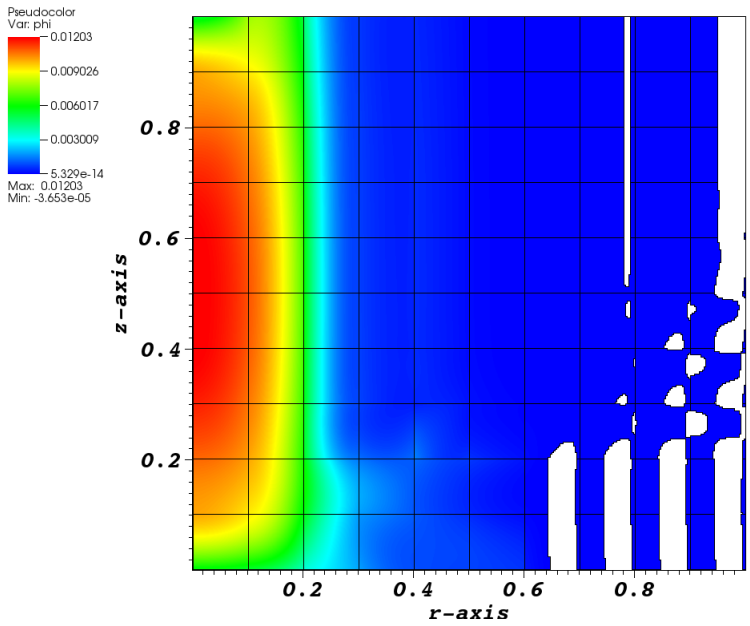

(a) Scalar flux.

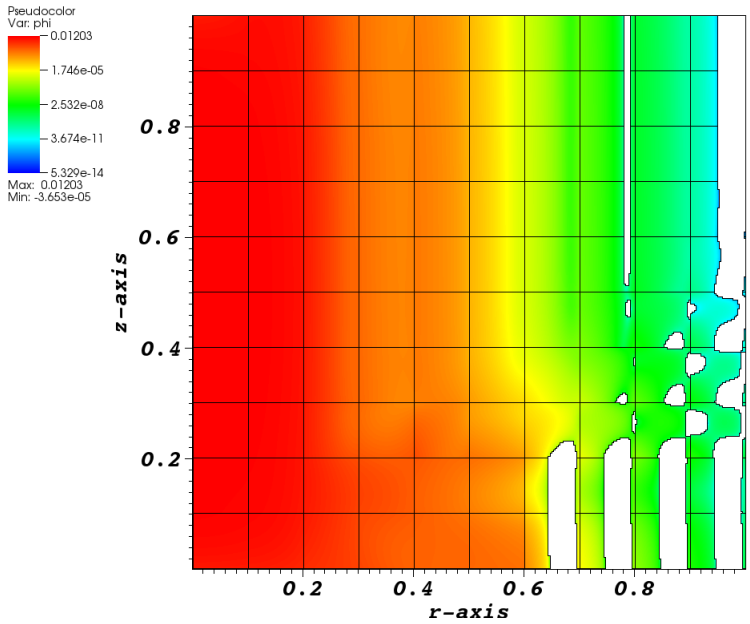

(b) Log of scalar flux.

Figure 9: Solution to multi-material stress test. White regions indicate negative scalar fluxes. This was solved without DSA and was only allowed 10,000 source iterations to complete.

1.8 Reflecting Boundary Conditions

To incorporate reflecting boundary conditions, we will "guess" the incident angular fluxes, update them with outgoing angular fluxes from the previous iteration, and adapt a convergence criterion for those fluxes. Along the z-axis, the reflection for direction $\mathbf{\Omega} = (\mu, \eta, \xi)$ is $\mathbf{\Omega}_R = (-\mu, \eta, \xi)$.

1.9 Reflecting Boundary Conditions

This may not warrant an entire subsection.

Reflecting boundaries are dependent upon the direction of the outgoing angular flux, $\mathbf{\Omega}_m$. The reflected incident direction is

$$\mathbf{\Omega}^R = \mathbf{\Omega}_m - 2\left(\mathbf{\Omega}_m \cdot \hat{n}\right)\hat{n} \tag{50}$$

where $\mathbf{\Omega}_m$ is the outgoing direction and $\hat{n}$ is the unit normal vector on the boundary (pointing outward). We apply a Dirichlet boundary condition for the angular flux in the reflected direction,

$$\psi^b(\boldsymbol{r}, \mathbf{\Omega}^R) = \psi_m \tag{51}$$